

Photoelectron Spectroscopy and Density Functional Investigation of the Structural Evolution, Electronic, and Magnetic Properties of CrSi_n^- ($n = 14-18$) Clusters

Kai Wang,[§] Hong-Yuan Zhao,[§] Lin Miao, Ze-Zhao Jia, Guang-Jia Yin, Xiao-Dong Zhu, Ramiro Moro, Bernd von Issendorff, and Lei Ma*



Cite This: *J. Phys. Chem. A* 2022, 126, 1329–1335



Read Online

ACCESS |



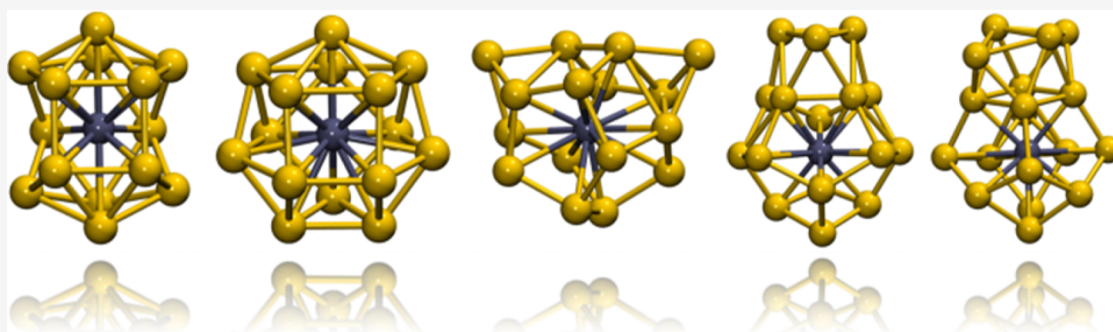
Metrics & More



Article Recommendations



Supporting Information



ABSTRACT: CrSi_n^- ($n = 14-18$) cluster anions have been investigated by a combination of photoelectron spectroscopy (PES) and first-principles calculations. The lowest-lying structures of the clusters have been determined by a global minimum search based on the genetic algorithm, combined with density functional theory (DFT) calculations. The simulated PES spectra of the lowest-energy isomers are in agreement with the experimental results, which gives strong evidence that the correct structures have been found. While sizes $n = 14$ and $n = 15$ prefer cage-like structures based on multi-center bonding within the cage, the larger sizes adopt structures based on fullerene-type cages around the Cr atom, with the additional atoms attached to the cage surface. A Hirshfeld analysis shows that the Cr atoms act as electron donors in all clusters, thus enhancing the electron count in the cage. It also reveals that the magnetic moment of $1\mu_B$ shown by all clusters is mainly contributed by the Cr atom. One interesting exception is size 17, where the Cr atom contributes a small moment antiparallel to that of the silicon cage.

1. INTRODUCTION

Insertion of transition metal (TM) atoms into pure silicon (Si) clusters may enhance their stability, possibly allowing them to be used for cluster-assembled materials with tailored properties for, e.g., the microelectronics industry.^{1,2} Owing to these potential applications in nanomaterials and semiconductors, this type of cluster system has been intensively studied by experiments and density functional theory (DFT) calculations over the past two decades.³⁻³³ Mass spectroscopy was employed first by Beck^{3,4} and later by the Lievens group⁵ to study the stability of TM (Cr, Mn, Cu, Mo, W)-doped Si clusters. The Nakajima group investigated the electronic properties of TM (Sc, Ti, V, Y, Zr, Nb, Hf, Ta)- and lanthanide metal (Tb, Ho, Lu)-doped silicon clusters using photoelectron spectroscopy (PES) and employed a combination of PES and mass spectroscopy to study the 3d-TM (Sc, Ti, V)-, 4d-TM (Y, Zr, Nb)-, and 5d-TM (Lu, Hf, Ta)-doped Si clusters.^{6,7} One of the important results was that TiSi_n clusters at $n = 16$ can exhibit both a high electronic and geometric stability, with the Si atoms forming a Frank–Kasper cage

around the Ti atom.⁷ Theoretical predictions for the structures and electronic properties of CrSi_n ($n = 8-16$),⁹ Si_nM ($n = 14-17$; $M = \text{Cr, Mo, and W}$),¹⁰ Si_nM ($M = \text{Sc}^-, \text{Ti, V}^+$; $n = 14-18$),¹¹ and M_2Si_{18} ($M = \text{Ti-Zn}$)¹² clusters have been reported in recent years. Zheng et al. systematically studied a series of TM (Sc, V, Cr, Co, Nb, Ag, Ta, Au)-doped sized Si_n^- clusters with $n \leq 14$ and CuSi_n^- for $n = 4-18$ by PES and first-principles calculations, leading to the identification of many ground-state structures.¹³⁻²⁵

To obtain data on CrSi_n^- for sizes beyond the closing of the first shell around the Cr atom, we have now performed PES measurements and DFT calculations on sizes $n = 14-18$.

Received: November 3, 2021

Revised: February 9, 2022

Published: February 17, 2022



2. EXPERIMENTAL AND THEORETICAL METHODS

2.1. Experimental Methods. The experiments were conducted in a magnetic-bottle PES apparatus equipped with a magnetron sputter gas aggregation cluster source, which has been described in detail elsewhere.^{34,35} Briefly, Cr and Si were sputtered from a sandwich-sputter target, consisting of a perforated silicon disk on top of a chromium one, into a liquid nitrogen-cooled gas mixture of helium and argon with a ratio of about 3:1 and a total pressure of about 0.5 mbar. Cr–Si cluster anions were guided by a hexapole radio-frequency ion guide to a radio-frequency 12-pole cryogenic ion trap cooled to 10 K. In the trap, the clusters were thermalized by collisions with helium buffer gas with a pressure of around 10^{-3} mbar. The Cr-doped Si clusters were extracted into a high resolution, double reflection time-of-flight mass spectrometer, where they were mass-selected by a multiwire mass gate with a resolution of about $m/\Delta m = 2000$ before being decelerated and irradiated by a 248 nm KrF laser beam in the interaction region of a magnetic-bottle type photoelectron spectrometer. The photoelectron spectra were averaged over 30,000 shots at a repetition rate of 100 Hz. The spectrometer was calibrated measuring the known PES of platinum anions, ensuring errors of the measured binding energies below 30 meV.

2.2. Theoretical Methods. The global search of the low-energy structures of CrSi_n^- ($n = 14\text{--}18$) was conducted using our own development of a genetic algorithm code combined with the ORCA program^{36,37} for energy calculations. The built-in BP86 functional³⁸ and the def2-SVP basis set^{39,40} were chosen to optimize each of the isomers obtained from the genetic algorithm code. For each size, more than 2000 configurations were computed to guarantee a high probability for locating the global minimum on the potential energy surface. The same functional with the def2-TZVP^{39,40} basis set was then used to further optimize the 10–30 lowest energy isomers obtained from the global search, and finally, the diffuse def2-TZVP (def2-TZVPD) basis set⁴¹ was employed to obtain even more accurate electronic energies, thus reinforcing the global minimum search. The resolution of the identity (RI) approximation⁴² was adopted in all calculations for better computing efficiency.

The VDE was calculated from the total energy difference between the anionic and neutral charge states of a cluster with the relaxed structure of the anionic state. Each line of the calculated Kohn–Sham (KS) eigenvalue spectrum was broadened by convolution with a Gaussian function with a FWHM of 0.06 eV to yield the simulated density of states (DOS), which was then shifted to align the binding energy of the highest-occupied KS orbital (HOMO) with the calculated VDE.⁴³

The cluster structures were rendered by the Visual Molecular Dynamics (VMD) software.⁴⁴ Hirshfeld population analysis was performed with the Multiwfn 3.8 (dev)⁴⁵ code based on the output results of the ORCA program.

3. RESULTS AND DISCUSSION

3.1. Photoelectron Spectra. The measured photoelectron spectra are displayed in Figure 1. One can observe that for sizes $n = 14$ and $n = 15$, there is a large separation between the highest, singly occupied state (marked X) and the next lower lying state (marked A), indicating a large bandgap between the highest occupied state (HOMO) and the lowest unoccupied state (LUMO) of the corresponding neutral cluster. This hints

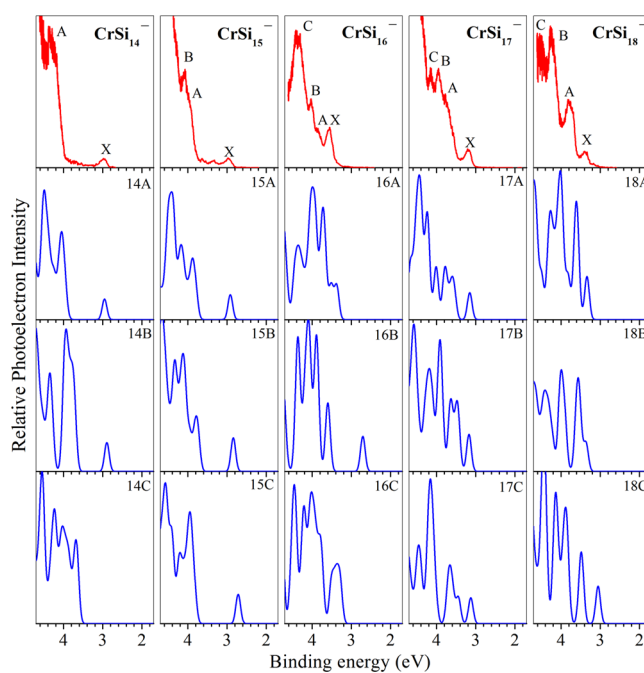


Figure 1. Uppermost panels: experimental PES spectra of cold CrSi_n^- ($n = 14\text{--}18$) measured at a photon energy of 5.01 eV. Lower panels: theoretical PES spectra calculated by density functional theory at the BP86/def2-TZVPD level for the structures shown in Figure 2.

at a high stability of these neutral clusters. For size 15, one can also observe two small peaks in the bandgap, which indicates the presence of a second isomer with a higher VDE and a smaller bandgap of the corresponding neutral cluster. Size $n = 16$ in contrast to the two smaller sizes exhibits a high VDE and a vanishing bandgap, as the high intensity of peak X indicates that more than one state is contributing to this peak. Sizes 17 and 18 are intermediate cases, with VDEs and bandgaps in between those of the two smallest sizes and size 16.

To obtain more information about these clusters, the lowest energy structures have been searched as described above. The results are shown in Figure 2. Here, for all sizes, the three lowest energy isomers identified by the extensive search are shown together with their calculated relative energies. The photoelectron spectra calculated for these structures are compared to the measured ones in Figure 1 (more structures and simulated spectra are displayed in the Supporting Information). Although the agreement is not perfect, the simulated spectrum of the respective lowest energy structure consistently exhibits the best agreement with the measured data. A special case here is size $n = 16$ again. Of all the low energy structures we found for this size, only structure 16A exhibits a vanishing bandgap. This means that it can be rather safely considered the structure present in the experiment despite that in the simulation peak, X is not really forming an isolated peak as in the experimental spectrum. Identifying the absolute minima of complex potential hypersurfaces is always a challenge, and there are notorious cases where the “catchment funnel” of the absolute minimum is so narrow that it is extremely difficult to find. However, even if the correct structure has been identified, correctly simulating a photoelectron spectrum strongly depends on the quality of the DFT calculation because different functionals predict slightly different bond lengths. In some cases (especially when there is a high density of states at the threshold, as in size 16), such

and more regular version of 15B. A structure close to 15A has already been predicted as the ground state geometry of neutral CrSi_{15} .²⁸ Structure 15C is another version of 15A; here, the triangular facet at the bottom of the cage has been rotated by 60° .

The ground state structure of size 16 is quite extraordinary. It can be seen as a heavily distorted version of the fullerene-like 14B, with one pentagonal facet capped by two Si atoms. It is close to a structure predicted for neutral MnSi_{16} .²⁸ What is quite surprising is that this somewhat irregular looking geometry is far more stable than any other geometry, with the next higher isomer 16B being less stable by 0.342 eV. The geometry of 16B is in fact a distorted version of a different fullerene cage, which consists of eight pentagons and two tetragons (instead of six pentagons and three tetragons as that of 14B). Like in structure 14C, one atom moved out of the fullerene cage, making it effectively a 15-atom cage capped by one Si atom. Structure 16C is 14B with a pentagonal facet capped by a Si dimer. With respect to other possible structures of this size, one should mention that the highly symmetric Frank–Kasper cage,²⁹ which is the ground state structure for ScSi_{16}^- , TiSi_{16} , and MnSi_{16}^+ ,¹¹ is not at all favorable for CrSi_{16} ; it has an energy 1.698 eV higher than the ground state. The high stability of this structure for the three systems mentioned above is in fact due to a combined geometric and electronic shell closure. For these, the embedded TM atoms formally donate four electrons to the system, which leads to a total valence electron count of 68 and a large bandgap between the occupied and unoccupied states.¹¹ Obviously, the structure still remains rather stable for one additional electron, like in $\text{CrSi}_{16}^{+8,26}$ or $\text{TiSi}_{16}^{-6,32}$, but becomes very unstable if two more electrons are added.

14B represents a building block for most of the larger clusters. Structures 17A, 17B, and 17C are all derived from 14B-based 16C, with a Si atom added to the capping Si dimer in different positions. Structure 18A is based on 14B again, with four atoms capping a tetragonal facet and one of the fullerene cage atoms popping out of the cage. Structure 18B is different as here, five atoms are capping a different fullerene, a distorted cage consisting of five tetragons and four pentagons, whereas 18C is 14B again with four atoms capping a pentagonal facet.

This means that almost all of the lower lying structures for the last three sizes consist of the fullerene cage 14B capped by additional atoms. This hints at a high stability of the cage, which is curious as 14B itself is not the lowest energy structure of the size 14 clusters. So, obviously, the fullerene cage gets further stabilized by this attachment of additional atoms.

3.3. Influence of the DFT Functional and Basis Set. It has been shown that the relative energies of TM-doped Si_{14} clusters strongly depend on the functional used.³¹ We therefore have tested other functionals as well, namely, PBE and PBE0, calculating the total energies for the structures optimized at the BP86/def2-TZVP level. The results are shown in Table 1.

One can see that the ground state structures determined with BP86 maintain the lowest energy structures also for the two other functionals. Nevertheless, the relative energies of the isomers as well as their energetic sequence strongly depend on the functional. One example is structure 14B, which is lower in energy than 14C for BP86 and only slightly above it for PBE, but is strongly disfavored for PBE0. It is also interesting that for all sizes except size 14, BP86 and PBE yield rather similar

Table 1. Relative Energies of the Different Structures Shown in Figure 2 for the Three Different Functionals^a

structures	relative energies (eV)		
	BP86	PBE	PBE0
14A	0.000	0.000	0.000
14B	0.199	0.519	0.565
14C	0.223	0.499	0.193
15A	0.000	0.000	0.000
15B	0.075	0.104	0.122
15C	0.159	0.208	0.209
16A	0.000	0.000	0.000
16B	0.342	0.371	0.589
16C	0.584	0.607	0.964
17A	0.000	0.000	0.000
17B	0.200	0.179	0.176
17C	0.265	0.318	0.316
18A	0.000	0.000	0.000
18B	0.132	0.181	0.283
18C	0.153	0.174	0.475

^aThe structures have been optimized at the BP86/def2-TZVP level; for the calculations, the basis set def2-TZVPD was used.

results; for size 14, however, the energies of the structures 14B and 14C are more than twice as large for PBE than for BP86, which indicates that PBE strongly favors structure 14A. As discussed in detail by Jin et al.,³¹ these differences have their origin in the different amounts of delocalization of the TM electrons predicted by the different functionals, which significantly stabilizes or destabilizes certain bonding motifs within the silicon cage.

In addition to this influence of the functionals in our calculations, we observe a strong dependence of the results on the basis sets employed, which has not been discussed so far. As a demonstration, we show in Figure 3 the energies of four structures of CrSi_{14}^- . Here, we chose the four isomers discussed by Yang et al.¹⁸ as they represent four different bonding motifs. These are, within our hierarchy of structures, the isomers 14A, 14B, 14C, and 14F. The first three structures have been discussed already; 14F (named 1D by Yang et al.) is a very regular geometry with D_{3d} symmetry, reminiscent of a slightly distorted bulk bcc lattice. To be able to refer to the results of Yang et al., who performed the calculations at the PBE/6-311+G(d) level, we also did test the calculations using PBE with different basis sets, namely, the Pople-type^{51–53} and Karlsruhe-type^{39–41} functions. The results are shown in Figure 3a,b, respectively. One can see that the sequence of the isomers for the Pople sets strongly depends on their quality, whereas for the Karlsruhe sets, convergence is already reached for def2-TZVP. To obtain the correct sequence (14A is much lower in energy than 14B, 14C, and 14F, which are almost degenerate) using Pople sets, it is obviously necessary to include the polarization basis functions at the G(2d) level, which means adding a second f-type function to the functions describing the Cr atom and a second d-type function to those of the Si atom. An interesting observation can be made when using different quality basis sets for the Si and Cr atoms: although the correct sequence is obtained when using the G(2d) level polarization functions for the Si atoms and G(d) level functions for the Cr atoms, this is not the case when it is done the other way around. This shows that, slightly against intuition, it is not the local electronic structure of the TM which requires a higher level treatment but instead that of the silicon atoms.

Presumably, this is due to the very different bonding patterns present in the different isomers—slight changes of the wavefunctions can therefore have quite a strong influence.

This result has to be taken as a caveat that for this type of system, not only the choice of the density functional is very important but that also rather high quality basis functions have to be used.

3.4. Cluster Properties. We will now discuss some of the calculated properties of the Cr-doped silicon cluster anions, namely, stabilities, VDEs, HOMO–LUMO gaps, and charge and spin localization.

For a CrSi_n^- cluster, the stability can be characterized by the average binding energy (E_b) defined as $E_b(\text{CrSi}_n^-) = [(n-1)E(\text{Si}) + E(\text{Si}^-) + E(\text{Cr}) - E(\text{CrSi}_n^-)]/(n+1)$, where $E(\text{CrSi}_n^-)$ is the energy of the anionic CrSi_n^- cluster; $E(\text{Si})$, $E(\text{Si}^-)$, and $E(\text{Cr})$ are the total energies of the neutral Si, anionic Si, and neutral Cr atoms, respectively. The average binding energies and HOMO–LUMO gaps of size $n = 14$ –18 are reported in Table 2 and plotted in Figure 5. The binding

Table 2. Data of Experimental (Expt.) and Theoretical (Theo.) Vertical Detachment Energies (VDEs), Binding Energies (E_b), the Second Order Energy Differences (Δ_2E) and HOMO–LUMO Gaps (Gap) of the CrSi_n^- ($n = 14$ –18) Clusters^a

clusters	VDE (eV)		E_b (eV)	gap (eV)	Δ_2E (eV)
	Expt.	Theo.			
CrSi_{14}^-	2.99(6)	2.95	3.835	0.731	
CrSi_{15}^-	2.98(6)	2.92	3.851	0.472	0.330
CrSi_{16}^-	3.55(6)	3.37	3.845	0.730	0.160
CrSi_{17}^-	3.20(6)	3.15	3.832	0.270	−0.266
CrSi_{18}^-	3.40(6)	3.34	3.833	0.373	

^aThe numbers in parentheses indicate the uncertainties.

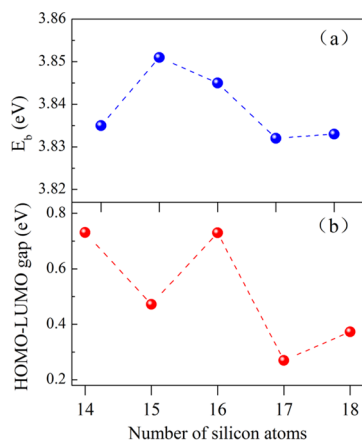


Figure 5. Binding energies E_b (a) and the HOMO–LUMO Gaps (b) of the CrSi_n^- ($n = 14$ –18) cluster anions as a function of cluster size.

energy varies only weakly with size, exhibiting a maximum at size $n = 15$ (Figure 5a). As seen in Figure 5b, the HOMO–LUMO gaps exhibit a clear odd–even alternation with respect to the number of silicon atoms; the odd-numbered CrSi_n^- clusters have a larger HOMO–LUMO gap than the neighboring even-sized ones. This is curious as all of the clusters have an odd number of valence electrons, which means that this cannot be an electron-pairing effect but has to have a more geometrical origin. CrSi_{14}^- and CrSi_{16}^- have the largest

HOMO–LUMO gaps of 0.731 and 0.730 eV, respectively, showing the high electronic stability of these clusters. To examine the relative stability, which for example determines the intensities of the different cluster sizes in mass spectra, the second order energy differences ($\Delta_2E = E_{n+1} + E_{n-1} - 2E_n$, where E_n is the total energy of CrSi_n^-) of the clusters in their ground state have been calculated and are shown in Table 2. Δ_2E also has a maximum at $n = 15$, indicating that the CrSi_{15}^- cluster possesses the largest relative stability.

To gain further insight into the electronic properties of the CrSi_n^- , the charge distribution was investigated with the Hirshfeld method. The charges on the Cr atom are displayed as a function of cluster size in Figure 6. They are +0.28 e, +0.30

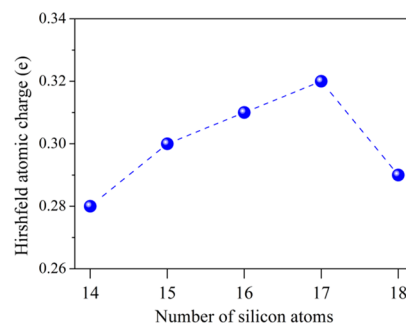


Figure 6. Hirshfeld atomic charges on the Cr atom for the CrSi_n^- ($n = 14$ –18) clusters.

e, +0.31 e, +0.32 e, and +0.29 e for $n = 14$ –18, indicating that the Cr atoms in these clusters act as electron donors, donating electrons to silicon cages.

Finally, we discuss the magnetic properties of the CrSi_n^- ($n = 14$ –18) clusters. To reveal their magnetic properties, a Hirshfeld population analysis was carried out for all cluster sizes, as presented in Table 3. It shows that the total magnetic

Table 3. Total Magnetic Moments (μ_T) of the CrSi_n^- Cluster Were Obtained by Hirshfeld Population Analysis along with the Local Magnetic Moment on the Cr Atom^a

clusters	CrSi_{14}^-	CrSi_{15}^-	CrSi_{16}^-	CrSi_{17}^-	CrSi_{18}^-
μ_T	1	1	1	1	1
μ_{Cr}	0.891	0.633	0.997	−0.195	0.660

^aAll magnetic moments are in μ_B .

moment of $1\mu_B$ of all clusters is mainly contributed by the Cr atom, except for $n = 17$. Here, the Cr atom has a magnetic moment antiparallel to that of the cage. We have seen such an antiparallel alignment also for other cluster structures, like 17B ($\mu_{\text{Cr}} = -0.22 \mu_B$). It seems to be the result of an interesting interplay of the geometric and electronic structures and certainly deserves further examination. These clusters could therefore be interesting candidates for gas phase X-ray absorption experiments, which are sensitive to the local electronic structure of the dopant atoms.⁵⁴

4. CONCLUSIONS

In summary, the geometric and electronic structures of the CrSi_n^- ($n = 14$ –18) have been systematically investigated by experimentally measured PES and density functional calculations. The calculated spectra are in agreement with the experimental spectra, corroborating the ground state structures

identified. The preferred structures for sizes $n = 14$ and 15 are closed cages with the chromium atom embedded inside, whereas larger clusters ($n \geq 16$) adopt structures based on a fullerene-type Si_{14} cage encapsulating the Cr atom, with extra Si atoms located on the surface of the cage. All clusters have a magnetic moment of $1\mu_B$, mainly contributed by the Cr atom. An exception is size 17 , where the Cr atom contributes a small moment antiparallel to the total moment. These results demonstrate that also for larger sizes, the TM-doped silicon clusters are very different from pure silicon clusters.

■ ASSOCIATED CONTENT

SI Supporting Information

The Supporting Information is available free of charge at <https://pubs.acs.org/doi/10.1021/acs.jpca.1c09557>.

More isomer structures and their simulated photoelectron spectra of CrSi_n^- ($n = 14-18$) are depicted in Figure S1 and Figure S2, respectively. The VDE values used five different functionals for the ground state of CrSi_n^- ($n = 14-18$) and are summarized in Table S1. The HOMO, VDE, and numerically determined asymptotic exchange-correlation shift of the clusters are shown in Table S2. The relative energies of the clusters for different SMs are shown in Table S3. The relative energies of the CrSi_{14}^- clusters for Pople-type and Karlsruhe-type basis sets are shown in Table S4. The relative energies of the clusters for Pople-type and Karlsruhe-type basis sets are listed in Tables S5 and S6 (PDF)

The Cartesian coordinates of the low-lying isomers of the CrSi_n^- clusters at the BP86/def2-TZVP level (ZIP)

■ AUTHOR INFORMATION

Corresponding Author

Lei Ma – Tianjin International Center for Nanoparticles and Nanosystems, Tianjin University, Tianjin 300072, China; orcid.org/0000-0002-2446-4833; Email: lei.ma@tju.edu.cn

Authors

Kai Wang – Tianjin International Center for Nanoparticles and Nanosystems, Tianjin University, Tianjin 300072, China

Hong-Yuan Zhao – Tianjin International Center for Nanoparticles and Nanosystems, Tianjin University, Tianjin 300072, China

Lin Miao – Tianjin International Center for Nanoparticles and Nanosystems, Tianjin University, Tianjin 300072, China

Ze-Zhao Jia – Tianjin International Center for Nanoparticles and Nanosystems, Tianjin University, Tianjin 300072, China

Guang-Jia Yin – Tianjin International Center for Nanoparticles and Nanosystems, Tianjin University, Tianjin 300072, China; orcid.org/0000-0002-9666-3719

Xiao-Dong Zhu – Tianjin International Center for Nanoparticles and Nanosystems, Tianjin University, Tianjin 300072, China

Ramiro Moro – Tianjin International Center for Nanoparticles and Nanosystems, Tianjin University, Tianjin 300072, China

Bernd von Issendorff – Fakultät für Physik, Universität Freiburg, D-79104 Freiburg, Germany; orcid.org/0000-0002-4358-4494

Complete contact information is available at:

<https://pubs.acs.org/10.1021/acs.jpca.1c09557>

Author Contributions

[§]K.W. and H.-Y.Z. contributed equally to this paper.

Notes

The authors declare no competing financial interest.

■ ACKNOWLEDGMENTS

This work was supported by the National Natural Science Foundation of China under Grant No. 11774255, the National Basic Research Program of China No. 2020YFC2004602, and the Key Project of National Science Foundation of Tianjin City No. 17JCZDJC30100.

■ REFERENCES

- (1) Koyasu, K.; Akutsu, M.; Mitsui, M.; Nakajima, A. Selective Formation of MSi_{16} ($M=\text{Sc, Ti, and V}$). *J. Am. Chem. Soc.* **2005**, *127*, 4998–4999.
- (2) Jena, P.; Sun, Q. Super Atomic Clusters: Design Rules and Potential for Building Blocks of Materials. *Chem. Rev.* **2018**, *118*, 5755–5870.
- (3) Beck, S. M. Studies of silicon cluster–metal atom compound formation in a supersonic molecular beam. *J. Chem. Phys.* **1987**, *87*, 4233–4234.
- (4) Beck, S. M. Mixed metal–silicon clusters formed by chemical reaction in a supersonic molecular beam: Implications for reactions at the metal/silicon interface. *J. Chem. Phys.* **1989**, *90*, 6306–6312.
- (5) Neukermans, S.; Wang, X.; Veldeman, N.; Janssens, E.; Silverans, R. E.; Lievens, P. Mass spectrometric stability study of binary MS_n clusters ($S=\text{Si, Ge, Sn, Pb}$, and $M=\text{Cr, Mn, Cu, Zn}$). *Int. J. Mass Spectrom.* **2006**, *252*, 145–150.
- (6) Koyasu, K.; Atobe, J.; Furuse, S.; Nakajima, A. Anion photoelectron spectroscopy of transition metal- and lanthanide metal-silicon clusters: MSi_n^- ($n=6-20$). *A. J. Chem. Phys.* **2008**, *129*, 214301.
- (7) Nakajima, A. Study on Electronic Properties of Composite Clusters toward Nanoscale Functional Advanced Materials. *Bull. Chem. Soc. Jpn.* **2013**, *86*, 414–437.
- (8) Palagin, D.; Gramzow, M.; Reuter, K. On the stability of non-magic endohedrally doped Si clusters: A first-principles sampling study of MSi_{16}^+ ($M=\text{Ti, V, Cr}$). *J. Chem. Phys.* **2011**, *134*, 244705.
- (9) Kawamura, H.; Kumar, V.; Kawazoe, Y. Growth, magic behavior, and electronic and vibrational properties of Cr-doped Si clusters. *Phys. Rev. B* **2004**, *70*, 245433.
- (10) Kumar, V.; Kawazoe, Y. Magic behavior of Si_{15}M and Si_{16}M ($M=\text{Cr, Mo, and W}$) clusters. *Phys. Rev. B* **2002**, *65*, No. 073404.
- (11) Torres, M. B.; Fernández, E. M.; Balbás, L. C. Theoretical study of isoelectronic Si_nM clusters ($M=\text{Sc}^-, \text{Ti, V}^+$; $n=14-18$). *Phys. Rev. B* **2007**, *75*, 205425.
- (12) Ji, W.; Luo, C. Structures, Magnetic Properties, and Electronic Counting Rule of Metals-Encapsulated Cage-Like M_2Si_{18} ($M = \text{Ti, Zn}$) Clusters. *Int. J. Quantum Chem.* **2011**, *112*, 2525–2531.
- (13) Xu, H. G.; Zhang, Z. G.; Feng, Y.; Zheng, W. Photoelectron spectroscopy and density-functional study of Sc_2Si_n^- ($n=2-6$) Clusters. *Chem. Phys. Lett.* **2010**, *498*, 22–26.
- (14) Xu, H. G.; Zhang, Z. G.; Feng, Y.; Yuan, J.; Zhao, Y.; Zheng, W. Vanadium-doped small silicon clusters: Photoelectron spectroscopy and density-functional calculations. *Chem. Phys. Lett.* **2010**, *487*, 204–208.
- (15) Huang, X.; Lu, S. J.; Liang, X.; Su, Y.; Sai, L.; Zhang, Z. G.; Zhao, J.; Xu, H. G.; Zheng, W. Structures and Electronic Properties of V_3Si_n^- ($n=3-14$) Clusters: A Combined Ab Initio and Experimental Study. *J. Chem. Phys. C* **2015**, *119*, 10987–10994.
- (16) Huang, X.; Xu, H. G.; Lu, S.; Su, Y.; King, R. B.; Zhao, J.; Zheng, W. Discovery of a silicon-based ferrimagnetic wheel structure

in $V_nSi_{12}^-$ ($x=1-3$) clusters: photoelectron spectroscopy and density functional theory investigation. *Nanoscale* **2014**, *6*, 14617–14621.

(17) Kong, X.; Xu, H. G.; Zheng, W. Structures and magnetic properties of $CrSi_n^-$ ($n = 3-12$) clusters: Photoelectron spectroscopy and density functional calculations. *J. Chem. Phys.* **2012**, *137*, No. 064307.

(18) Yang, B.; Xu, H.; Xu, X.; Zheng, W. Photoelectron Spectroscopy and Theoretical Study of $Cr_nSi_{15-n}^-$ ($n=1-3$): Effects of Doping Cr Atoms on the Structural and Magnetic Properties. *J. Phys. Chem. A* **2018**, *122*, 9886–9893.

(19) Lu, S. J.; Cao, G. J.; Zheng, W. J. The structural and electronic properties of $NbSi_n^{-/0}$ ($n = 3-12$) clusters: anion photoelectron spectroscopy and ab initio calculations. *Nanoscale* **2016**, *8*, 19769–19778.

(20) Lu, S. J.; Xu, H. G.; Xu, X. L.; Zheng, W. J. Anion Photoelectron Spectroscopy and Theoretical Investigation on $Nb_2Si_n^{-/0}$ ($n = 2-12$) Clusters. *J. Phys. Chem. C* **2017**, *121*, 11851–11861.

(21) Kong, X. Y.; Deng, X. J.; Xu, H. G.; Yang, Z.; Xu, X. L.; Zheng, W. J. Photoelectron spectroscopy and density functional calculations of $AgSi_n^-$ ($n = 3-12$) clusters. *J. Chem. Phys.* **2013**, *138*, 244312.

(22) Lu, S. J.; Xu, X. L.; Xu, H. G.; Zheng, W. J. Structural evolution and bonding properties of $Au_2Si_n^{-/0}$ ($n = 1-7$) clusters: Anion photoelectron spectroscopy and theoretical calculations. *J. Chem. Phys.* **2018**, *148*, 244306.

(23) Yang, B.; Xu, X. L.; Xu, H. G.; Farooq, U.; Zheng, W. J. Structural evolution and electronic properties of $CoSi_n^-$ ($n = 3-12$) clusters: mass-selected anion photoelectron spectroscopy and quantum chemistry calculations. *Phys. Chem. Chem. Phys.* **2019**, *21*, 6207–6215.

(24) Lu, S. J.; Xu, H. G.; Xu, X. L.; Zheng, W. J. Structural Evolution and Electronic Properties of $TaSi_n^{-/0}$ ($n = 2-15$) Clusters: Size-Selected Anion Photoelectron Spectroscopy and Theoretical Calculations. *J. Phys. Chem. A* **2020**, *124*, 9818–9831.

(25) Xu, H. G.; Wu, M. M.; Zhang, Z. G.; Yuan, J.; Sun, Q.; Zheng, W. Photoelectron spectroscopy and density functional calculations of $CuSi_n^-$ ($n = 4-18$) clusters. *J. Chem. Phys.* **2012**, *136*, 104308.

(26) Lau, J.; Hirsch, K.; Klar, P.; Langenberg, A.; Lofink, F.; Richter, R.; Rittmann, J.; Vogel, M.; Zamudio-Bayer, V.; Möller, T.; et al. X-ray spectroscopy reveals high symmetry and electronic shell structure of transition-metal-doped silicon clusters. *Phys. Rev. A* **2009**, *79*, No. 053201.

(27) Abreu, M. B.; Reber, A. C.; Khanna, S. N. Does the 18-Electron Rule Apply to $CrSi_{12}$? *J. Phys. Chem. Lett.* **2014**, *5*, 3492–3496.

(28) Wang, J.; Ma, Q. M.; Xu, R. P.; Liu, Y.; Li, Y. C. 3d transition metals: Which is the ideal guest for Si_n ($n = 15, 16$) cages? *Phys. Lett. A* **2009**, *373*, 2869–2875.

(29) Kumar, V.; Kawazoe, Y. Metal-Encapsulated Fullerene-like and Cubic Caged Clusters of Silicon. *Phys. Rev. Lett.* **2001**, *87*, No. 045503.

(30) Ohara, M.; Koyasu, K.; Nakajima, A.; Kaya, K. Geometric and electronic structures of metal (M)-doped silicon clusters ($M=Ti, Hf, Mo$ and W). *Chem. Phys. Lett.* **2003**, *371*, 490–497.

(31) Jin, X.; Arcisauskaitė, V.; McGrady, J. E. The structural landscape in 14-vertex clusters of silicon, $M@Si_{14}$: when two bonding paradigms collide. *Dalton Trans.* **2017**, *46*, 11636–11644.

(32) Wu, X.; Du, Q.; Zhou, S.; Huang, X.; Chen, M.; Miao, L.; Yin, G.; Wang, J.; Wang, K.; von Issendorff, B.; et al. Structures, stabilities and electronic properties of $Ti_mSi_n^-$ ($m = 1-2, n = 14-20$) clusters: a combined ab initio and experimental study. *Eur. Phys. J. Plus* **2020**, *135*, 734.

(33) Zhao, J.; Du, Q.; Zhou, S.; Kumar, V. Endohedrally Doped Cage Clusters. *Chem. Rev.* **2020**, *120*, 9021.

(34) Ma, L.; Issendorff, B. v.; Aguado, A. Photoelectron spectroscopy of cold aluminum cluster anions: Comparison with density functional theory results. *J. Chem. Phys.* **2010**, *132*, 104303.

(35) Xue, W.; Liang, X.; Du, Q.; Zhao, J.; Chen, M.; Miao, L.; Wang, J.; Yin, G.; Ma, L.; King, R. B.; et al. Medium-sized Si_n^- ($n=14-20$)

clusters: a combined study of photoelectron spectroscopy and DFT Calculations. *J. Phys.: Condens. Matter* **2018**, *30*, 354002.

(36) Neese, F. The ORCA program system. *WIREs Comput. Mol. Sci.* **2012**, *2*, 73–78.

(37) Neese, F. Software update: the ORCA program system, version 4.0. *WIREs Comput. Mol. Sci.* **2017**, *8*, No. e1327.

(38) Perdew, J. P. Density-functional approximation for the correlation energy of the inhomogeneous electron gas. *Phys. Rev. B* **1986**, *33*, 8822.

(39) Weigend, F.; Ahlrichs, R. Balanced Basis Sets of Split Valence, Triple Zeta Valence and Quadruple Zeta Valence Quality for H to Rn: Design and Assessment of Accuracy. *Phys. Chem. Chem. Phys.* **2005**, *7*, 3297–3305.

(40) Weigend, F. Accurate Coulomb-fitting basis sets for H to Rn. *Phys. Chem. Chem. Phys.* **2006**, *8*, 1057–1065.

(41) Rappoport, D.; Furche, F. Property-optimized Gaussian basis sets for molecular response calculations. *J. Chem. Phys.* **2010**, *133*, 134105.

(42) Neese, F. An Improvement of the Resolution of the Identity Approximation for the Formation of the Coulomb Matrix. *J. Comput. Chem.* **2003**, *24*, 1740–1747.

(43) Akola, J.; Manninen, M.; Häkkinen, H.; Landman, U.; Li, X.; Wang, L. S. Photoelectron spectra of aluminum cluster anions: Temperature effects and ab initio simulations. *Phys. Rev. B* **1999**, *60*, R11297–R11300.

(44) Humphrey, W.; Dalke, A.; Schulten, K. VMD: Visual molecular dynamics. *J. Mol. Graph.* **1996**, *14*, 33–38.

(45) Lu, T.; Chen, F. Multiwfn: A multifunctional wavefunction analyzer. *J. Comput. Chem.* **2012**, *33*, 580–592.

(46) Perdew, J. P.; Burke, K.; Ernzerhof, M. Generalized Gradient Approximation Made Simple. *Phys. Rev. Lett.* **1996**, *77*, 3865.

(47) Adamo, C.; Barone, V. Toward Reliable Density Functional Methods without Adjustable Parameters: The PBE0 Model. *J. Chem. Phys.* **1999**, *110*, 6158.

(48) Becke, A. D. Density-functional exchange-energy approximation with correct asymptotic behavior. *Phys. Rev. A* **1988**, *38*, 3098–3100.

(49) Lee, C.; Yang, W.; Parr, R. G. Development of the Colle-Salvetti Correlation-Energy Formula into a Functional of the Electron Density. *Phys. Rev. B* **1988**, *37*, 785–789.

(50) Becke, A. D. Density Functional Thermochemistry. III. The Role of Exact Exchange. *J. Chem. Phys.* **1993**, *98*, 5648.

(51) Dobbs, K. D.; Hehre, W. J. Molecular orbital theory of the properties of inorganic and organometallic compounds 5. Extended basis sets for first-row transition metals. *J. Comput. Chem.* **1987**, *8*, 861–879.

(52) Gordon, M. S.; Binkley, J. S.; Pople, J. A.; Pietro, W. J.; Hehre, W. J. Self-consistent molecular-orbital methods. 22. Small split-valence basis sets for second-row elements. *J. Am. Chem. Soc.* **1982**, *104*, 2797–2803.

(53) Rassolov, V. A.; Pople, J. A.; Ratner, M. A.; Windus, T. L. 6-31G* basis set for atoms K through Zn. *J. Chem. Phys.* **1998**, *109*, 1223.

(54) Zamudio-Bayer, V.; Leppert, L.; Hirsch, K.; Langenberg, A.; Rittmann, J.; Kossick, M.; Vogel, M.; Richter, R.; Terasaki, A.; Möller, T.; et al. Coordination-Driven Magnetic-to-Nonmagnetic Transition in Manganese-Doped Silicon Clusters. *Phys. Rev. B* **2013**, *88*, 115425.